AIAA JOURNAL
Vol. 34, No. 10, October 1996

Effect of Fences on Airfoil Aerodynamics at −90 Degree Incidence

Paul M. Stremel*
NASA Ames Research Center, Moffett Field, California 94035

A two-dimensional computational method is applied to accurately calculate the viscous flow about airfoils normal to the freestream flow. In particular, the flow about an XV-15 wing airfoil with an upper or lower surface fence at −90 deg incidence is evaluated. A parametric study is conducted to investigate and understand the effect of fences on the flow about an airfoil normal to the freestream flow. This investigation includes the effect of fence location for both upper and lower surfaces and of fence height on airfoil aerodynamic characteristics. Comparisons of the time-averaged lift, drag, pitching moment, and surface pressure distributions are made to evaluate the effectiveness of each airfoil/fence configuration. The results indicate that 1) the airfoil drag is highly dependent on the fence chordwise location, ranging from a 15% increase in drag for an upper surface fence to a 35% decrease in drag for a lower surface fence with respect to the basic airfoil value; 2) the airfoil drag is also dependent on the fence height, with a drag reduction of 25% for a lower surface fence of 35% chord height located at 15% chord; and 3) the reduction in drag is the direct result of decreased pressure on the airfoil upper surface near the leading edge and an increase in the lower surface pressure over the entire airfoil chord.

Nomenclature

C_d = sectional drag coefficient, Drag/$(\frac{1}{2}\rho U^2 c \cdot 1)$
C_l = sectional lift coefficient, Lift/$(\frac{1}{2}\rho U^2 c \cdot 1)$
C_m = sectional moment coefficient, computed at 0.25c = Moment/$(\frac{1}{2}\rho U^2 c^2 \cdot 1)$
C_p = pressure coefficient $= (p - p_\infty)/(\frac{1}{2}\rho U^2)$
c = airfoil chord length for undeflected flap
h = fence height
n_η, n_ξ = vector length in transformed space
p = pressure
Re = Reynolds number, Uc/ν
t = time
U = freestream velocity
u = local velocity component in x direction
u_η, u_ξ = transformed velocity component
v = local velocity component in y direction
x, y = Cartesian coordinates
α = incidence angle
η, ξ = coordinates in transformed space
ν = kinematic viscosity
ρ = density
ω = vorticity

Subscript

∞ = value at far field

Introduction

THE numerical prediction of download, the drag produced by rotorcraft during hover, is of considerable importance in the design analysis of rotorcraft. The flowfield beneath the rotor is complex because of the three-dimensional flowfield dominated by the rotor wake. In hover the flowfield is complicated further in that the rotor wake interacts directly with flow along the surface of the fuselage or other vehicle components (i.e., rotor blades, forward fuselage, tail boom). Download limits helicopter performance in hover and is a significant problem in the design of tilt-rotor configurations. For tilt-rotor configurations in hover, the lifting wing is immersed in the rotor wake normal to the downwash, severely limiting the hover performance of the aircraft.[1] The ability to predict this phenomenon would be very beneficial and could provide a means for limiting the effect of the rotor wake on the wing, providing for improved hover performance.

One possible method for reducing the drag on airfoils normal to the freestream flow is the inclusion of plates or fences extending from the airfoil surface parallel to the freestream flow (Fig. 1). The flow over an airfoil at −90 deg incidence is depicted in Fig. 1a and is characterized by a separated wake below the airfoil. The separated wake is composed of alternating leading and trailing edge vortices, which influence the lower surface pressure on the airfoil. The ability to alter the developing separated wake can be highly beneficial in controlling the airfoil lower surface pressure and, therefore, reducing drag. A fence extending into the wake (Fig. 1b), represents an extension to the splitter plate technique. The effect of the splitter plate is to control the development of the separated vortices in the wake of

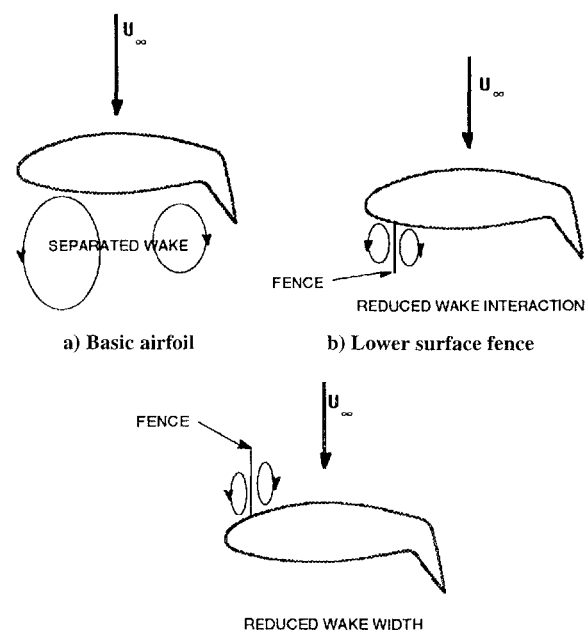

a) Basic airfoil b) Lower surface fence

c) Upper surface fence

Fig. 1 Effect of fences on airfoil flowfield.

Received Aug. 5, 1995; revision received June 4, 1996; accepted for publication June 5, 1996.

*Aerospace Engineer, Applied Computational Aerodynamics Branch, Applied Aerodynamics Divison.

the body and to effectively streamline the body, resulting in reduced drag.[2] Alternately, a fence can be extended into the oncoming flow, as in Fig. 1c. The effect of this upstream fence is again to streamline the body and to reduce the overall width of the shed wake behind the body, thereby reducing the drag. The use of upstream fences in drag reduction on a noncircular cylinder is reported in Ref. 3. In that study, the drag on a noncircular cylinder with a flat freestream facing surface was reduced by as much as 81% with the use of upstream fences.

A two-dimensional method was previously developed to calculate the flow about bluff bodies.[4] Results have also been obtained for airfoils with and without a deflected flap at −90 deg incidence.[5] Additionally, the effect of Reynolds number and turbulence have been computed for the XV-15 wing airfoil with and without a deflected flap.[6] The results of Ref. 6 indicate that the flowfield solution is highly Reynolds number and turbulence dependent. Excellent correlation between prediction and test were obtained when matching the test Reynolds number and incorporating the Baldwin–Barth turbulence model.[7] This correlation provides confidence in using the current method as a tool to further investigate the reduction of drag on airfoils at −90 deg incidence.

The intent of this paper is to explore and understand the effect of fences on the flow about an airfoil normal to the freestream flow. This includes an investigation to determine the effect of fence location for both upper and lower surfaces and of fence height on airfoil aerodynamic characteristics. Comparisons of time-averaged lift, drag, pitching moment, and surface pressure distributions are made to evaluate the effectiveness of each airfoil/fence configuration. Instantaneous streamlines and pressure distributions representative of the shedding of the leading and trailing edge vortices are also presented.

Numerical Method

The flowfield is modeled by the velocity/vorticity form of the unsteady, incompressible Navier–Stokes equations. The governing equations in two-dimensional Cartesian coordinates are written, for the continuity equation,

$$\frac{\partial u}{\partial x} + \frac{\partial v}{\partial y} = 0 \tag{1}$$

the vorticity transport equation,

$$\frac{\partial \omega}{\partial t} + \frac{\partial (u\omega)}{\partial x} + \frac{\partial (v\omega)}{\partial y} = \nu \nabla^2 \omega \tag{2}$$

and the definition of vorticity,

$$\omega = \frac{\partial v}{\partial x} - \frac{\partial u}{\partial y} \tag{3}$$

with $\nabla^2 = \partial^2(\,)/\partial x^2 + \partial^2(\,)/\partial y^2$.

A body-fitted computational mesh is used in the finite difference model of the governing equations. A portion of the computational mesh is shown in Fig. 2. The Cartesian equations are transformed into the computational domain (ξ, η), and the governing equations become as follows:

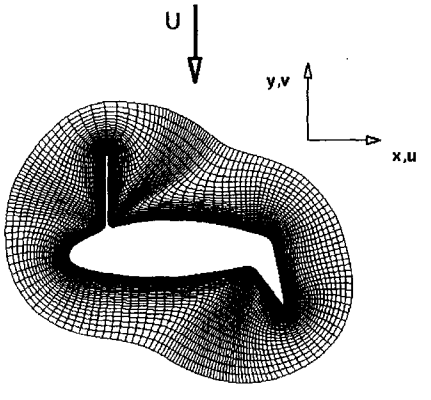

Fig. 2 Computational grid.

For the continuity equation,

$$\left[\frac{\partial (n_\eta u_\xi)}{\partial \xi} + \frac{\partial (n_\xi u_\eta)}{\partial \eta}\right] \Big/ (n_\xi n_\eta) = 0 \tag{4}$$

for the vorticity transport equation,

$$\frac{\partial \omega}{\partial t} + \left[\frac{\partial (n_\eta u_\xi \omega)}{\partial \xi} + \frac{\partial (n_\xi u_\eta \omega)}{\partial \eta}\right] \Big/ (n_\xi n_\eta)$$

$$= \nu \left\{\frac{\partial}{\partial \xi}\left[\left(\frac{n_\eta}{n_\xi}\right)\frac{\partial \omega}{\partial \xi}\right] + \frac{\partial}{\partial \eta}\left[\left(\frac{n_\xi}{n_\eta}\right)\frac{\partial \omega}{\partial \eta}\right]\right\} \Big/ (n_\xi n_\eta) \tag{5}$$

and for the definition of vorticity,

$$\omega = \left[\frac{\partial (n_\eta u_\eta)}{\partial \xi} - \frac{\partial (n_\xi u_\xi)}{\partial \eta}\right] \Big/ (n_\xi n_\eta) \tag{6}$$

where

$$n_\xi = \left(x_\xi^2 + y_\xi^2\right)^{\frac{1}{2}}, \qquad n_\eta = \left(x_\eta^2 + y_\eta^2\right)^{\frac{1}{2}}$$

The solution is obtained by solving the finite difference representations of the governing equations using a staggered-grid methodology.[6] The boundary conditions are calculated implicitly as part of the solution, thereby fully coupling the vorticity and velocity. The boundary conditions for the transformed governing equations at the airfoil surface are calculated from the no-slip condition as

$$u_\xi = 0, \qquad u_\eta = 0 \tag{7}$$

The boundary condition for the surface vorticity is calculated implicitly as part of the solution from Eq. (6). The boundary conditions at the far-field boundary are set to the freestream values in the potential flow region upstream of the airfoil and computed from the governing equations to allow convection of vorticity out of the computational domain downstream of the airfoil. The turbulent model used in this method is a modified version of the Baldwin–Barth one-equation model.[7] This model solves a single advection-diffusion-source term equation for the eddy viscosity. The eddy viscosity is added to the kinematic viscosity to obtain the total viscosity for the flow. The surface pressure is calculated by an integral method outlined in Ref. 8.

The flow is started impulsively. An impulsive start requires that the flowfield velocity be equal to the potential flow except at the airfoil surface, where the velocity is zero, and the initial distribution of surface vorticity is calculated from this potential-velocity field. The flowfield solution at each time step after the impulsive start is obtained by a single inversion of the block-tridiagonal coefficient matrix. The solution is not iterated, and the conservation of mass is computed to machine zero at each time step. The solution is then advanced by updating the flowfield variables and solving the flow for the next time step. The solution is terminated at a desired time or after sufficient time has elapsed for the demonstration of flowfield periodicity.

This method has been applied previously to an airfoil for correlation purposes. A sample of these results will be presented in the next section. Then results for numerous airfoil/fence configurations to determine the effect of fence location and height on airfoil aerodynamic properties will be presented. Results presented include airfoil lift, drag, pitching moment, surface pressure distributions, and flowfield streamlines.

Results and Discussion

Prior to computing the flow for the XV-15 airfoil with fences, the flow for the basic airfoil at −90 deg incidence was computed. The airfoil geometry includes a 30% trailing edge flap deflected to 60 deg. The flow was calculated for a Reynolds number of 1×10^6 while modeling turbulent flow. The results are compared with measured XV-15 airfoil pressure data[9] in Fig. 3. The comparison is shown to be quite good in that the method predicts accurately the lower surface pressure and the negative pressure peak on the upper surface near the flap hinge location. Additional comparisons can be found in Ref. 6.

To understand the effectiveness of fences in reducing airfoil drag, a parametric study of the XV-15 wing airfoil with fences at −90 deg incidence was conducted. The effect of fence height and location

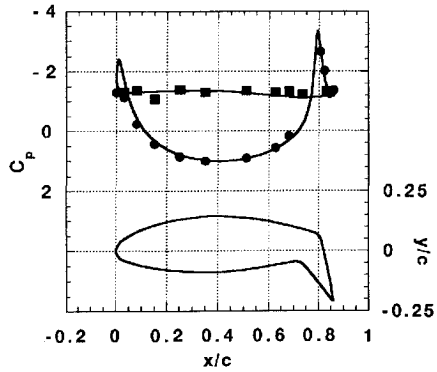

Fig. 3 Comparison of predicted time-averaged surface pressure with experiment: $\alpha = -90$ deg, $\delta_f = 60$ deg, $Re = 1 \times 10^6$; ——, computed; •, upper surface, exp.; and ■, lower surface, exp.

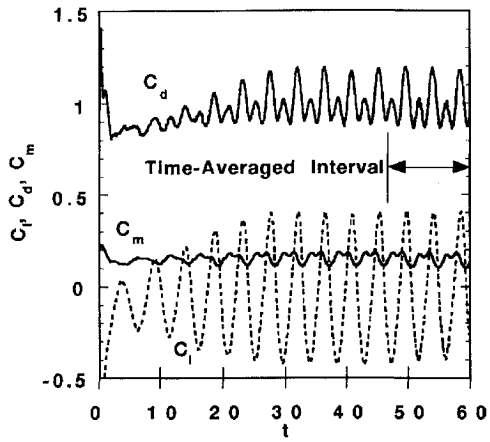

Fig. 4 Time-dependent lift, drag, and pitching moment: lower surface fence, $x/c = 0.15$, $h/c = 0.3$.

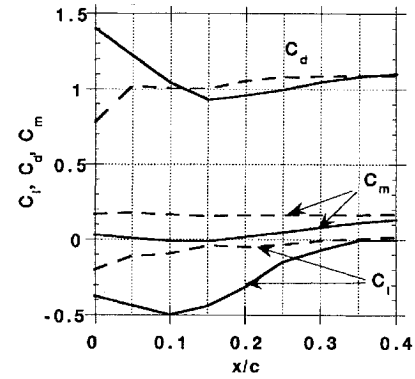

Fig. 5 Effect of fence location on time-averaged lift, drag, and pitching moment; upper or lower surface fence, $h/c = 0.3$: ——, upper surface fence and – – –, lower surface fence.

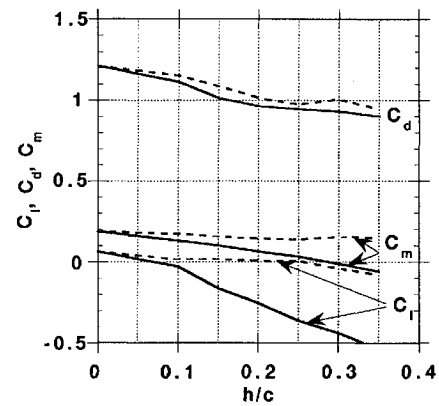

Fig. 6 Effect of fence height on time-averaged lift, drag, and pitching moment; upper or lower surface fence, $x/c = 0.15$: ——, upper surface fence and - - - -, lower surface fence.

on the airfoil aerodynamics was computed. Fences on the airfoil upper and lower surface were considered. The time-averaged lift, drag, and pitching moment are presented next, followed by surface pressure and streamlines to understand the effect of the fences on the flowfield.

Time-Averaged Lift, Drag, and Pitching Moment

The time-averaged lift, drag, and pitching moment are computed by averaging the time-dependent lift, drag, and pitching moment over an interval of time equal to three cycles of vortex shedding. A single cycle of vortex shedding is defined as an interval of time over which a leading and trailing edge vortex are shed. A sample of the time-dependent lift, drag, and pitching moment is shown in Fig. 4, as is the time-averaged interval. The lift, drag, and pitching moment are traditionally defined, with positive lift normal to the freestream flow (toward the airfoil trailing edge; Fig. 2), positive drag parallel to the freestream flow, and a positive pitching moment tending to increase the incidence.

Effect of Chordwise Fence Location, Upper or Lower Surface Fence

The effect of the chordwise fence location was computed for a fence height $h/c = 0.30$ while considering a single upper or lower surface fence. The variations in the time-averaged lift, drag, and pitching moment on the airfoil are shown in Fig. 5. The basic airfoil lift, drag, and pitching moment, without a fence, are equal to $C_l = 0.066$, $C_d = 1.212$, and $C_m = 0.190$, respectively. Figure 5 shows significant differences in the airfoil drag when the results are compared for an upper or lower surface fence located at the leading edge of the airfoil. The upper surface fence increases the airfoil drag by 15% with respect to the basic airfoil drag. In contrast, the effect of a lower surface fence located at the leading edge of the airfoil is to reduce the drag by 35% with respect to the basic airfoil drag. As the fence is moved aft on the airfoil, the benefit in drag reduction of the lower surface fence is greatly reduced, and the drag is reduced for the upper surface fence. The effect of the upper surface fence is ultimately to reduce the drag of the airfoil by 25% with respect to the basic airfoil, when the fence is positioned at $x/c = 0.15$. The lower surface fence reduces the drag by 20% with respect to the basic airfoil at this location. Only small variations in the pitching moment are shown to be the effect of the upper or lower surface fence. Large reductions in lift with respect to the basic airfoil value are shown for an upper surface fence located near the leading edge, especially when located at $x/c = 0.1$.

Effect of Fence Height, Upper or Lower Surface Fence at $x/c = 0.15$

The effect of fence height was computed for a fence location of $x/c = 0.15$ while considering a single upper or lower surface fence. The variations in the time-averaged lift, drag, and pitching moment on the airfoil are shown in Fig. 6. A steady decrease in the airfoil drag is shown for increasing fence height. This is shown for both the upper and lower surface fence results, with a slight improvement in drag reduction for the upper surface fence when compared to the drag for the lower surface fence. Results were not computed for fence heights greater than $h/c = 0.35$. A reduction in drag of 25% with respect to the basic airfoil drag is shown for an upper surface fence of height $h/c = 0.35$. A steady decrease in the lift and pitching moment is shown for increasing fence height. These variations in the lift and pitching moment are significant for the upper surface fence results, while only small changes are shown for the lower surface fence results.

Effect of Fence Height, Lower Surface Fence at $x/c = 0.0, 0.15$

The variations in the time-averaged lift, drag, and pitching moment for a lower surface fence located at $x/c = 0.0$ and 0.15 are shown in Fig. 7. Only small variations in the drag reduction are shown up to a fence height of $h/c = 0.1$. For a fence height greater than $h/c = 0.1$ but less than $h/c = 0.2$, almost identical drag reduction (approximately 20%) is shown for both lower surface fence

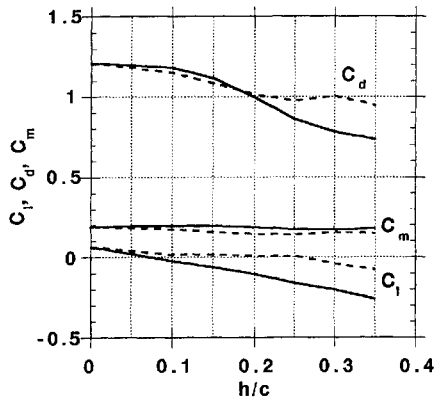

Fig. 7 Effect of fence height and location on time-averaged lift, drag, and pitching moment; lower surface fence: ——, fence at x/c = 0.0 and - - - - -, fence at x/c = 0.15.

locations. For a fence height greater than $h/c = 0.2$, a continued drag reduction is shown when the lower surface fence is located at the leading edge, while only a small further reduction in drag is shown for the fence located at $x/c = 0.15$. There is virtually no variation in the pitching moment as a result of fence height and only small differences when comparing the results for the different fence locations. However, a large decrease in lift is shown for a fence located at the airfoil leading edge when compared to the results for a fence located at $x/c = 0.15$.

These significant variations in the airfoil lift, drag, and pitching moment result from the effect of the fences on the flowfield and, hence, the airfoil surface pressure. The results for the airfoil surface pressure will be described next.

Time-Averaged Surface Pressure

An examination of the time-averaged surface pressure distributions is presented to better understand the variations in the airfoil lift, drag, and pitching moment due to fence location. The time-averaged pressure distributions for a fence located on the upper or lower surface, at the leading edge or $x/c = 0.15$, and of height $h/c = 0.3$ are presented. These chordwise locations represent the most significant variations in the airfoil drag as shown in Fig. 5. The time-averaged surface pressure on the airfoil is computed by averaging the time-dependent surface pressure over an interval of time equal to three cycles of vortex shedding. This interval in time is identical to the one used to compute the time-averaged lift, drag, and pitching moment on the airfoil and is shown in Fig. 4. The effect of chordwise fence location on the airfoil average pressure distribution is shown in Figs. 8 and 9 for an upper or lower surface fence, respectively.

In Fig. 8 the variation in the time-averaged surface pressure is shown for an upper surface fence located at the airfoil leading edge and $x/c = 0.15$. Also shown are the results for the basic airfoil for comparison. When the upper surface fence is located at the airfoil leading edge, the upper surface pressure is increased to the stagnation pressure value, $C_p = 1.0$, over 40% of the chord. There is also increased pressure on the lower surface over the same area. This increased pressure on the lower surface will decrease the airfoil drag with respect to the basic airfoil drag. However, the overall drag is increased because of the increased upper surface pressure. The increase in the lower surface pressure typifies diminished separated wake interaction with the flow near the airfoil lower surface. When the fence is located at $x/c = 0.15$ on the upper surface, a separation bubble is formed forward of the fence. This is shown in Fig. 8 as a region of negative pressure toward the leading edge of the fence location. The significant drag reduction for this fence location is the result of the increased lower surface pressure over the entire airfoil chord.

The variation in the airfoil-average-surface pressure for a lower surface fence located at the airfoil leading edge and $x/c = 0.15$ is shown in Fig. 9. The decreased drag associated with the lower surface fence results from the significant decrease in pressure on the upper surface of the airfoil near the leading edge and an increase in the lower surface pressure over the entire airfoil chord. The increased

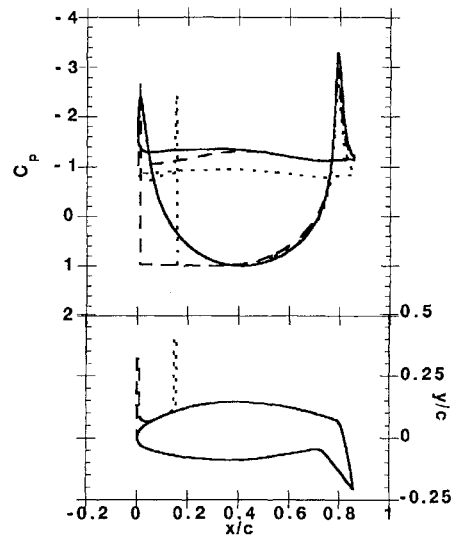

Fig. 8 Effect of fence location on time-averaged surface pressure; upper surface fence, h/c = 0.3: ——, basic airfoil; – – –, fence at x/c = 0.0; and - - - - -, fence at x/c = 0.15.

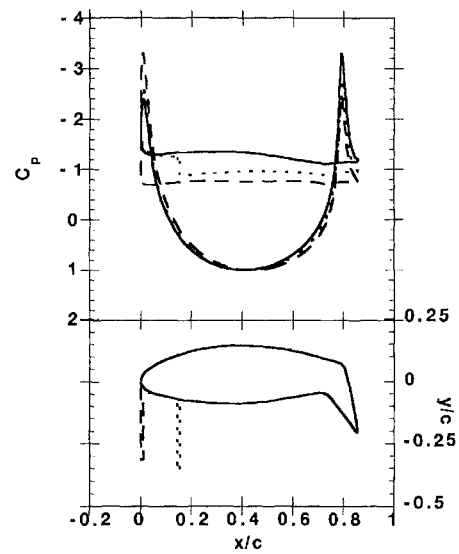

Fig. 9 Effect of fence location on time-averaged surface pressure; lower surface fence, h/c = 0.3: ——, basic airfoil; – – –, fence at x/c = 0.0; and - - - - -, fence at x/c = 0.15.

lower surface pressure indicates that the influence of the separated wake on the flow near the airfoil lower surface has been reduced. When the lower surface fence is moved aft to $x/c = 0.15$, the formation of a lower surface separation bubble between the leading edge and the fence location is indicated by the decreased surface pressure at that location. The lower surface pressure is also increased with respect to the basic airfoil value, although not to the degree that it is when the fence is located at the airfoil leading edge.

Flowfield Streamlines

Flowfield streamlines are presented for an upper or lower surface fence located at the airfoil leading edge. The fence height is equal to $h/c = 0.30$. These two configurations were chosen because they represent extremes in the airfoil drag as shown in Fig. 5. Because the drag on the airfoil is dependent on the shedding of a leading or trailing edge vortex (Fig. 4), time-averaged streamlines are inappropriate for isolating the effect of a fence on the flowfield. Rather, the instantaneous streamlines are presented at times for local minimum and maximum lift on the airfoil. These times also represent a local maximum in drag on the airfoil (Fig. 4). When the lift is at a local minimum, toward the airfoil leading edge, a leading edge vortex is being shed. In contrast, a local maximum in lift represents the shedding of a trailing edge vortex.

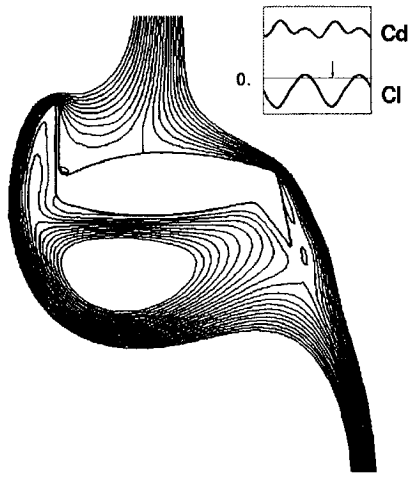

Fig. 10a Instantaneous streamlines for leading edge vortex development; upper surface fence at airfoil leading edge, $h/c = 0.3$.

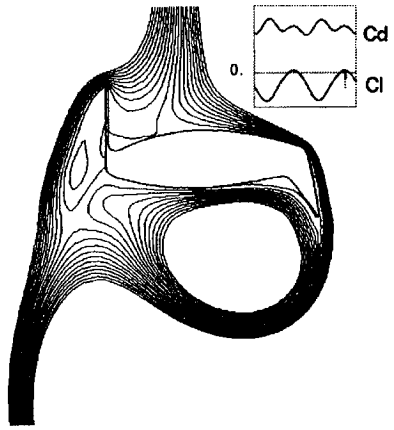

Fig. 10b Instantaneous streamlines for trailing edge vortex development; upper surface fence at airfoil leading edge, $h/c = 0.3$.

The flowfield streamlines for an upper surface fence during the shedding of a leading edge vortex and a trailing edge vortex are shown in Figs. 10a and 10b, respectively. An insert is included in each figure depicting the time-dependent lift and drag on the airfoil. Shown in the insert is a marker indicating the point during the lift and drag history at which the instantaneous streamlines are shown. In Fig. 10a the lift is at a local minimum and, therefore, a leading edge vortex is being shed. This is clearly shown by the concentric streamlines in the figure. The streamlines for the trailing edge vortex are shown in Fig. 10b. Here again the separated vortex is shown on the figure by the concentric streamlines below the airfoil. When comparing the lift and drag histories in the inserts, the airfoil drag is shown to be greater during the leading edge vortex development than for the trailing edge vortex. This is the result, in part, of the relative position of the leading and trailing edge vortices with respect to the lower surface of the airfoil and the influence of the vortices on the lower surface pressure. This is shown in the instantaneous surface pressure distributions of Fig. 11. Shown in the figure are the surface pressure distributions representative of the streamlines shown in Figs. 10a and 10b for the leading and trailing edge vortices, respectively. The results indicate the main contribution to the reduced drag, when comparing the drag for the trailing edge vortex to that for the leading edge vortex, is not the result of differences in the lower surface pressure, but rather of differences in the upper surface pressure. While the average lower surface pressure varies little between the cases, the upper surface pressure is reduced significantly during the trailing edge vortex development, resulting in the reduced drag.

The flowfield streamlines for a lower surface fence during the shedding of a leading edge vortex and a trailing edge vortex are shown in Figs. 12a and 12b, respectively. An insert is again included

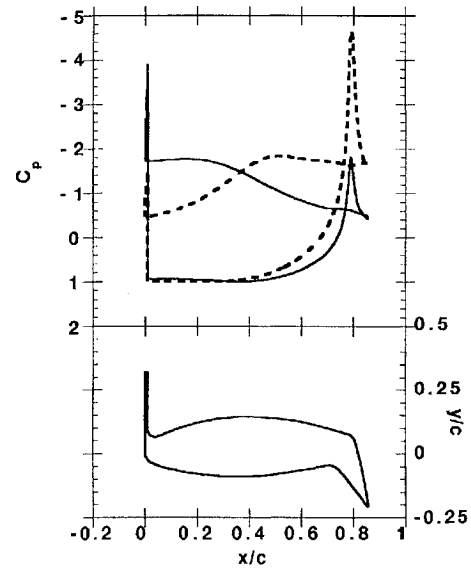

Fig. 11 Instantaneous surface pressure, upper surface fence at airfoil leading edge, $h/c = 0.3$: ——, leading edge vortex and - - - - -, trailing edge vortex.

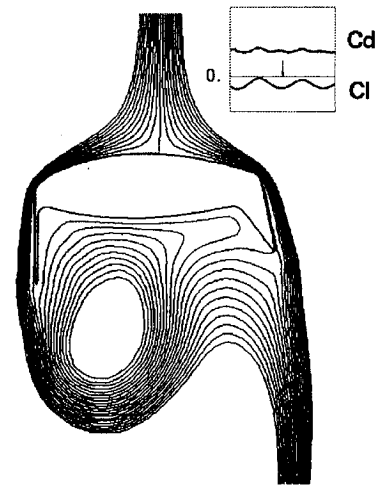

Fig. 12a Instantaneous streamlines for leading edge vortex development; lower surface fence at airfoil leading edge, $h/c = 0.3$.

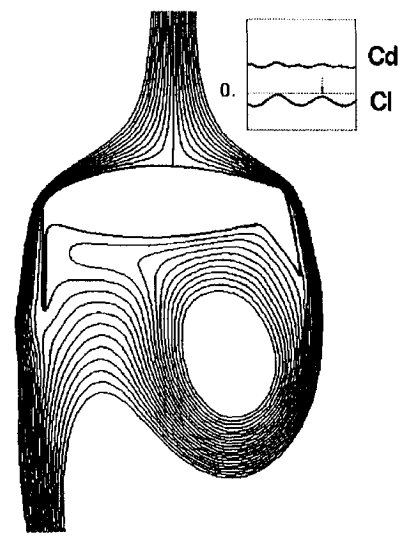

Fig. 12b Instantaneous streamlines for trailing edge vortex development; lower surface fence at airfoil leading edge, $h/c = 0.3$.

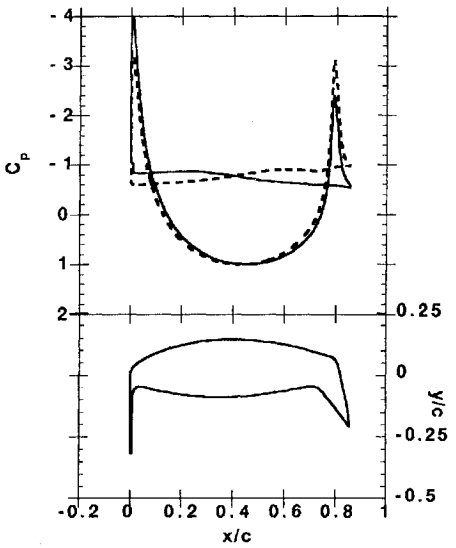

Fig. 13 Instantaneous surface pressure; lower surface fence at airfoil leading edge, $h/c = 0.3$: ——, leading edge vortex; and - - - -, trailing edge vortex.

in each figure depicting the time-dependent lift and drag on the airfoil. A marker indicates the point during the lift and drag history at which the instantaneous streamlines are shown. In Fig. 12a the lift is at a local minimum and, therefore, a leading edge vortex is being shed. This is clearly shown by the concentric streamlines. The streamlines for the trailing edge vortex are shown in Fig. 12b. Here again the separated vortex is shown by the concentric streamlines below the airfoil.

In comparing the lift and drag histories in the inserts of Figs. 12a and 12b with those of Figs. 10a and 10b, the airfoil drag is shown to be decreased significantly, which was also shown in the time-averaged drag in Fig. 5. In addition, the oscillation amplitude of the lift and drag are reduced when compared to those of Figs. 10a and 10b. These results indicate that the lower surface fence not only reduces significantly the drag, when compared to the upper surface fence results, but also reduces the unsteady wake effects on the airfoil lift and drag. This is further demonstrated in the instantaneous surface pressure distributions of Fig. 13. The surface pressure is shown to be less dependent on the separated wake, when compared to the pressure for the upper surface fence (Fig. 11).

Conclusions

A two-dimensional computational method has been applied to calculate the influence of upper or lower surface fences on airfoil aerodynamics. In particular, the flow about an XV-15 airfoil with a 30% trailing edge flap deflected 60 deg at −90 deg incidence was considered. The flow was calculated for a Reynolds number of 1×10^6 while modeling turbulent flow. Results were computed to determine the effect of fence height, upper or lower surface location, and chordwise location on the lift, drag, pitching moment, and surface pressure distribution. The results indicate the following:

1) The lift, drag, and pitching moment are highly dependent on the fence chordwise location. This is demonstrated for a fence height of $h/c = 0.3$ for both an upper and a lower surface fence.

a) When an upper surface fence is located at the leading edge, the drag is increased by 15% with respect to the basic airfoil value. However, when the upper surface fence is located at $x/c = 0.15$, the drag is reduced by 25% with respect to the basic airfoil value.

b) In contrast, a lower surface fence located at the airfoil leading edge reduces the drag by 35% with respect to the basic airfoil value. When the lower surface fence is located at $x/c = 0.15$, the drag is reduced by 20% with respect to the basic airfoil value.

2) The lift, drag, and pitching moment are also dependent on the fence height. When comparing the results for an upper or lower surface fence located at $x/c = 0.15$, a steady decrease in airfoil drag is shown for increasing fence height, up to a drag reduction of 25% at $h/c = 0.35$. The drag reduction for an upper or lower surface fence is nearly identical as a function of fence height.

3) The instantaneous streamlines and surface pressure distributions are highly dependent on the shedding of the leading and trailing edge vortices for an upper surface fence located at the airfoil leading edge. In contrast, the effect of a lower surface fence located at the airfoil leading edge is to minimize the effect of the shed wake on the surface pressure distribution, thereby reducing the oscillations in the lift and drag resulting from the periodic shedding of the leading and trailing edge vortices.

References

[1]Wood, T. L., and Peryea, M. A., "Reduction of Tiltrotor Download," *American Helicopter Society 49th Annual Forum* (St. Louis, MO), American Helicopter Society, 1993, pp. 1177–1191.

[2]Hoerner, S. F., *Fluid-Dynamic Drag*, Author, Brick Town, NJ, 1965.

[3]Pamadi, B. N., Pereira, C., and Laxmana Gowda, B. H., "Drag Reduction by Strakes of Noncircular Cylinders," *AIAA Journal*, Vol. 26, No. 3, 1988, pp. 292–299.

[4]Stremel, P. M., "Calculation of Flow about Two-Dimensional Bodies by Means of the Velocity–Vorticity Formulation on a Staggered Grid," AIAA Paper 91-0600, Jan. 1991.

[5]Stremel, P. M., "Calculation of Unsteady Airfoil Loads With and Without Flap Deflection at −90 Degrees Incidence," AIAA Paper 91-3336, Sept. 1991.

[6]Stremel, P. M., "The Effect of Reynolds Number and Turbulence on Airfoil Aerodynamics at −90 Degrees Incidence," AIAA Paper 93-0206, Jan. 1993.

[7]Barth, T. J., "Numerical Aspects of Computing Viscous High Reynolds Number Flows on Unstructured Meshes," AIAA Paper 91-0721, Jan. 1991.

[8]Wang, C. M., Wu, J. C., and Tuncer, I. H., "Accurate Determination of Surface Pressure in High Reynolds Number Flows," First International Conf. on Computational Methods in Flow Analysis, Okayama, Japan, Sept. 1988.

[9]Maisel, M. D., Laub, G. H., and McCroskey, W. J., "Aerodynamic Characteristics of Two-Dimensional Wing Configurations at Angles of Attack Near −90 Degrees," NASA TM-88373, Dec. 1986.